Performing optical logic operations on linear polarization modes using diffractive deep neural networks

Shuqing Chen,[1,†] Chaowen Tian,[1,†] Zebin Huang,[1,†] Wenjie Xiong,[1] Jiafu Chen,[1] Peipei Wang,[2] Huapeng Ye,[3] Ying Li,[1,*] and Dianyuan Fan[1]

[1] *International Collaborative Laboratory of 2D Materials for Optoelectronics Science and Technology of Ministry of Education, Institute of Microscale Optoelectronics, Shenzhen University, Shenzhen 518060, China*

[2] *School of Physics and Electronic Information, Huaibei Normal University, Huaibei, 235000, China*

[3] *Guangdong Provincial Key Laboratory of Optical Information Materials and Technology & Institute of Electronic Paper Displays, South China Academy of Advanced Optoelectronics, South China Normal University, Guangzhou 510006, China*

(Received 6 December 2023; revised 10 March 2024; accepted 15 May 2024; published 11 June 2024)

Optical logic operations are pivotal for optical signal processing and digital computing, enabling rapid parallel computation. However, traditional optical logic operations often adhere to the electronic logic paradigm, representing logic variables based on intensity distribution. These methods contain limitations regarding the range of logic functions and energy consumption. Herein, we introduce linear polarization (LP) modes as optical logic variables, offering a departure from these constraints by harnessing the weakly coupled processing of the two-dimensional asymmetric spatial distribution of LP modes. The weak coupling mechanism within LP modes empowers the diffractive deep neural network (D^2NN) to accomplish coupling conversion between lateral and longitudinal components. This not only surmounts the limitations in conventional LP mode processing but also significantly enhances the degree of modulation freedom with minimal energy loss. Through establishing linear mapping relationships for input and output LP mode vectors, our study demonstrates that a three-layered D^2NN successfully executes fundamental logical operations (AND, OR, and NOT) alongside combined logic operations (NAND and NOR). Numerical results showcase a diffraction efficiency exceeding 92%, with mode purity surpassing 97%. In addition, by integrating AND and OR logic operations within a single D^2NN, we achieve modal purity exceeding 97%. These findings confirm the potential of employing the D^2NN for logical operations on weakly coupled LP modes, offering promising avenues for precise manipulation of other intricate modal fields.

DOI: 10.1103/PhysRevApplied.21.064025

I. INTRODUCTION

Optical logic operations [1–4] play a pivotal role in optical digital computing [5–8] and signal processing [9–12], promising high-speed, broad-bandwidth data processing capabilities. However, conventional optical logic operations have been heavily influenced by the principles from electrical logic operations, where amplitude serves as the primary representation of logic variables [1,13]. These optical logic operation techniques typically rely on nonlinear operations and manipulation of various light properties to precisely modulate amplitude parameters in input optical signals. In electronics, the amplitude of electrical signals can be modulated by directly controlling current or voltage. Nevertheless, amplitude modulation in optics faces limitations in logic functionality and results in high energy consumption due to linear [14–16] and nonlinear [17,18] interference effects and transmission losses. Previous research aimed at modulating phase parameters through multibeam interference to convert the phase shifts of signal light into amplitude modulation, enabling partial all-optical logic operations. However, these methods have limitations in logic capabilities and efficiencies due to the finite phase modulation range and sensitivity to environmental disturbances. Leveraging its capability for profound feature information extraction and all-optical information processing, the diffractive deep neural network (D^2NN) has been deployed for the modulation and demodulation of orbital angular momentum (OAM) modes [19–21]. A novel strategy utilizing OAM modes for optical logical operations was recently introduced [22], showcasing the execution of seven basic logic operations and the integration of half-adder logic operations, illustrating their practicality. This innovative approach provided a new solution for optical logic operations. OAM modes, distinguished by their mode orthogonality and limitless

*Corresponding author: queenly@szu.edu.cn
†Authors contributed equally to this paper

 © 2024 American Physical Society

dimensionality, facilitate intricate spatial encoding within optical computing by manipulating the phase information within their circular configurations. This capability is essential for stable signal transmission and precise outcome evaluation, broadening the possibilities for executing multivalued logic operations [22]. In contrast, linear polarization (LP) modes, inherent to optical fibers, have become commonly used due to their ability to accommodate a broader range of orthogonal modes within a specific radius. LP modes, serving as the intrinsic modes of optical fibers, offer superior compatibility with fiber transmission and on-chip integration when contrasted with orbital angular momentum (OAM) modes characterized by ring structures. LP modes are advantageous as they support a broader spectrum of orthogonal modes within a specified radius. Their two-dimensionally asymmetric structures furnish additional degrees of freedom, enabling the design of a more diverse array of logic functions. This capability effectively addresses the limitations of traditional optical logic operations, which rely on modulating parameters such as amplitude and phase, and often suffer from restricted logical functionalities and low efficiencies [11,13,23]. Harnessing the complete spatial structure of LP modes holds the promise of enhancing channel capacity, facilitating more intricate spatial logic encoding, and introducing innovative design principles to the field of optical computing.

In this context, we introduce a weakly coupled strategy for the orthogonal transformation of LP modes, leveraging diffractive deep neural networks [24–33]. This approach enables the conversion between lateral and longitudinal components of LP modes. The mutilayered diffractive structure within the D^2NN facilitates independent modulation of input light fields by progressively manipulating the phase wave fronts. This establishes a high-dimensional mapping relationship between input and output light fields. The incorporated deep learning architecture [34–38] aids in accurately computing the desired phase or amplitude distributions for the multilayered diffractive structure, proving highly effective in various applications including logical operations [19], image processing [39,40], (de)multiplexing [41], and more. Manipulating the two-dimensional asymmetric field structure of LP modes and establishing diverse mapping relationships are crucial aspects of the logic operation mechanism. The orthogonality between the lateral and longitudinal dimensions of LP modes enables the D^2NN to implement weak coupling mechanisms via a progressive wave front modulation, granting independent control over the radial and angular dimensions. This results in abundant modulation functions capable of accommodating various complex logic controls, overcoming the limitations of finite logic functionalities. Furthermore, the linear mapping relationship established by the multistage diffractive structure between mode manipulation and modulation functions allows for a low-loss LP mode conversion, effectively addressing the issue of high energy loss. In terms of optical implementation, the orthogonal transformation of weakly coupled LP modes can be achieved through phase modulation and free-space diffraction. It can be sequentially approximated by multiplication of multiple phase and diffraction matrices. By propagating the error backward, the matrix parameters can be iteratively optimized to achieve linear conversion between orthogonal mode groups.

To validate the proposed logic operation mechanism for LP modes, we successfully demonstrated logical operations in simulations using three-layer D^2NNs. These operations include AND, OR, NOT, NAND, and NOR, all achieved with over 92% diffraction efficiency and 97% modal purity. In addition, we implemented integrated logic AND and OR operations among four higher-order LP modes (LP_{02}, LP_{03}, LP_{11}, and LP_{12}), achieving mode purity exceeding 97%. These results confirm the viability of utilizing the D^2NN for logical operations on weakly coupled LP modes. This strategy can be extended to precisely manipulate other complex modal fields. The adoption of LP modes to encode logic constants represents a significant breakthrough, overcoming the limitations of traditional intensity-based representations. The multifunctionality and low power characteristics of LP mode waveguide control open the door to various on-chip integration possibilities, which could significantly advance the development of optical computing and optical signal processing.

II. PRINCIPLES AND METHODS

The principle of weakly coupling LP mode orthogonal transformation is depicted in Fig. 1. Orthogonal transformations within finite-dimensional product spaces maintain the matrix norm of vectors, allowing for the conversion between input and output vectors. The mathematical conversion of two orthogonal vectors can be achieved by

$$v_1 = O v_2 O^{\dagger}, \tag{1}$$

where $O^{\dagger}$ represents the complex conjugate transpose matrix. By leveraging the norm-preserving property of orthogonal transformations and expanding their modulation dimension, LP mode vectors with orthogonality can be utilized instead of vectors. Furthermore, by expanding the modulation dimension to n, a mapping relationship can be established to simultaneously convert LP modes, i.e.,

$$\begin{bmatrix} E_{out\_1} \\ \vdots \\ E_{out\_n} \end{bmatrix} = O \begin{bmatrix} E_{in\_1} \\ \vdots \\ E_{in\_n} \end{bmatrix} O^{\dagger}. \tag{2}$$

For the two-dimensional asymmetric structure of the LP mode, the lateral and longitudinal components of the input

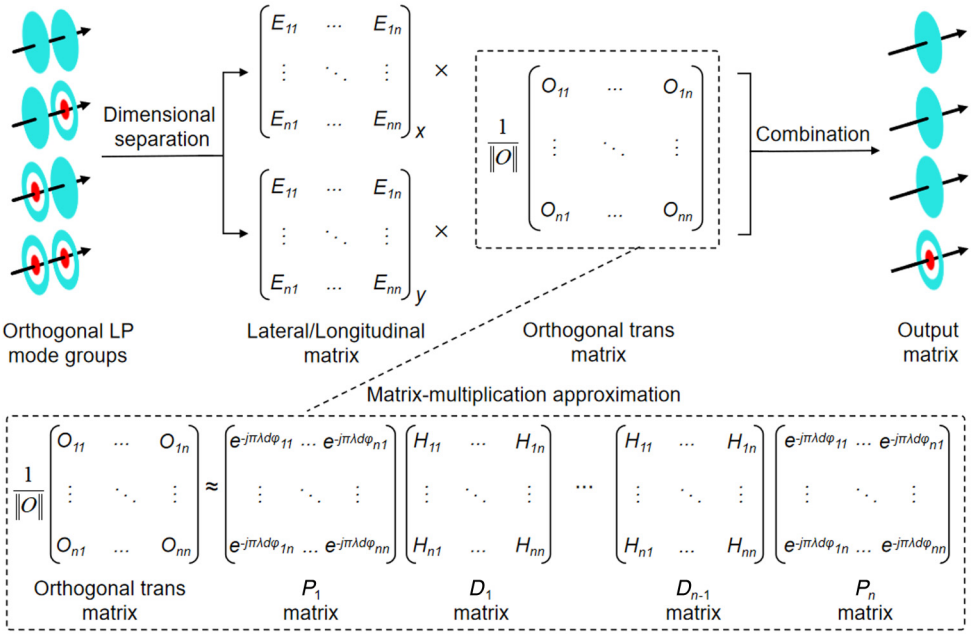

FIG. 1. Orthogonal transformation of the LP mode groups with dimensional separation and combination modulations. Here, D_{n-1} represents the diffraction $(n-1)$ matrix and P_n is the phase n matrix.

LP mode can be separated and subjected to orthogonal transformation processing individually. The D^{2}NN processes the lateral and longitudinal components of the input LP mode by multiplying them with the transfer matrix of each diffraction layer. It then couples the new lateral and longitudinal components as outputs for each layer. This approach demonstrates high diffraction efficiency as it utilizes orthogonal matrices for transformation, thus avoiding deterioration in the amplitude distribution in the x- or y-direction of the field, leading to

$$E_{out\_1} = O[E_{in\_1x} + E_{in\_1y}]O^{\dagger}. \tag{3}$$

Moreover, this orthogonal transformation can employ singular value decomposition to obtain a common solution through the approximate of multiple linear transformation matrices, i.e.,

$$O \times E_{in} \times O^{\dagger} \approx H^n \varphi^n \cdots H^2 \varphi^2 H^1 \varphi^1 E_{in}, \tag{4}$$

where H represents the Fresnel diffraction matrix defined in the frequency domain, conforming to the propagation law of interlayer secondary waves; φ stands for a phase modulation matrix that preserves the norm of the matrix. This illustrates that the orthogonal transformation of weakly coupled LP mode can be accomplished through phase modulation and free-space diffraction.

The physical realization of the D^{2}NN model involves multiple diffractive surfaces. It integrates deep learning techniques with error backpropagation methods, possessing both the learning ability of traditional artificial neural networks and the modulation capability of optical fields. In this model, each pixel on every diffractive layer is treated as an artificial neuron within a neural network. Every pixel manipulates the incident light wave, establishing an optical diffractive connection with artificial neurons on other layers. According to the Huygens principle, each point on a specific layer functions as a secondary source for the light wave. As an artificial neuron, it connects to other neurons on the subsequent layer, undergoing complex modulation of phase initiated by the preceding layer. The propagation and superposition of interlayer secondary waves adhere to the following principle:

$$\omega^L(f_x, f_y) = \exp\left(\frac{j2\pi d_L}{\lambda}\right) \exp[j\pi\lambda d_L(f_x^2 + f_y^2)], \tag{5}$$

where (f_x, f_y) denotes the spatial frequency at the (x, y) point on the Lth diffraction layer, d_L represents the distance between layers, j signifies the imaginary unit, and λ is the working wavelength. The expression for the output of the Lth diffraction layer is as follows:

$$Y^L = F^{-1}[F(U^L)\omega^L], \tag{6}$$

where F and F^{-1} represent the Fourier transform and inverse Fourier transform, respectively; U^L is determined by the input wave and transmission coefficient. Typically, the phase of each neuron is an adjustable parameter, allowing for complex modulation at each layer, thereby enhancing the inference performance of the diffractive neural network. In this context, we perform logical operation

functions by providing training data at the input layer and then outputting the results through the D^2NN. We iteratively train the phase values of the D^2NN neurons at each layer. The transmission or reflection coefficients of neurons across all specified layers of the D^2NN are established after the training. Detailed information concerning the gradient descent algorithm can be found in Appendix A. Its advantages lie in its fast computing speed and low power consumption.

III. RESULTS AND ANALYSIS

We constructed the D^2NN model using optical diffraction theory and the error backpropagation algorithm, which includes an input layer, three optical diffraction layers, and an output layer. The model is equipped with adjustable phase values to execute LP mode logical operations. The input dataset encompasses four states: "00", "01", "10", and "11". These represent specific input optical fields arranged in LP_{01} and LP_{02} mode combinations for logical operations. When applied to binary logic gates, these four input states yield logic state responses "0" or "1" (determined by the logic gate rules) subsequent to phase modulation across three layers of optical diffraction. Figure 2 represents the schematic diagram illustrating the optical field processing within the three-layer D^2NN.

The D^2NN model independently modulates the central incident optical field, which comprises two LP modes originating from the same spatial position. Following phase modulation and diffracted transmission across three optical diffraction layers, the LP mode is emitted from the center of the output screen. Conversely, the operational principle of the logic NOT gate differs from other logic gates. Its input port solely requires one LP mode, representing the two input states "0" and "1". Further elaboration on this aspect will be provided below.

We begin with the design of the LP mode logic AND gates. The training dataset for the D^2NN comprises four superimposed optical fields, with the first column illustrating the complex distribution of the input beam. Here, A and B denote two logical variables that can assume either of two modes (i.e., LP_{01} and LP_{02}). Hence, the output of the logical operations can be represented as

$$Y = f\,(A, B), \tag{7}$$

where f signifies the logical operation function. The expected output of the logical AND gate is depicted in Fig. 3. The logic operation follows $Y = AB$.

Initially, we input these four input data samples into the three-layer D^2NN model and continuously updated and adjusted the phase distribution across the diffraction layers to minimize the loss function. This process aimed to bring the D^2NN model's prediction results closer to the ideal outcomes, consequently enhancing the accuracy and generalization capability of the model. Throughout the iterative training, the network's loss value declined rapidly initially and then stabilized gradually. After 5000 iterations, the D^2NN model ultimately converges, and the loss function approaches zero. This convergence highlights our D^2NN mode's capability to handle multiple LP modes, precisely resolve the diffraction structure within each layer, and autonomously modulate the four input optical fields. Given that both input and output beams reside in the central position of the diffraction layer, the essential information primarily concentrates at this central point.

Since the D^2NN model is trained to handle four distinct input states, the resulting logic AND gate accurately responds and modulates all of these states without altering the diffraction structure. Figure 4 illustrates the diffraction efficiency and mode purity of the AND logical operation. The diffraction efficiency, quantifying the energy loss in

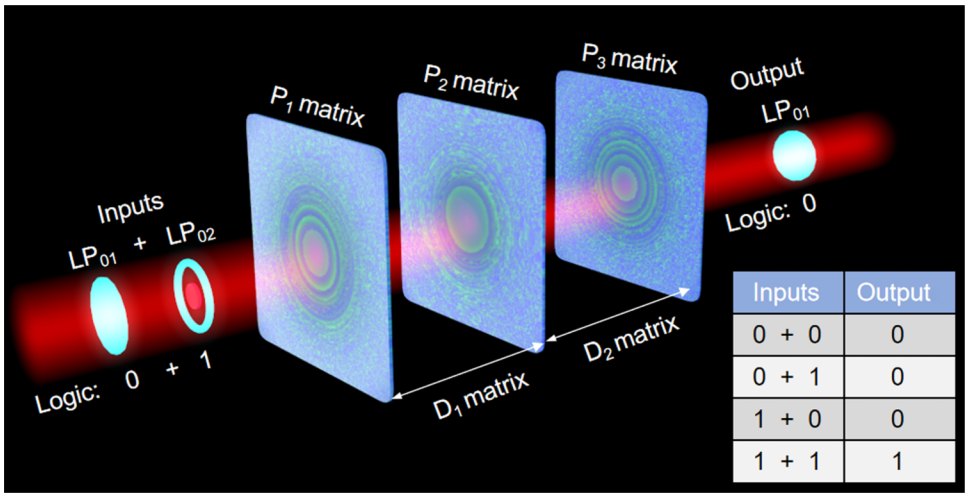

FIG. 2. Optical implementation of the LP mode logic operations with diffractive deep neural networks.

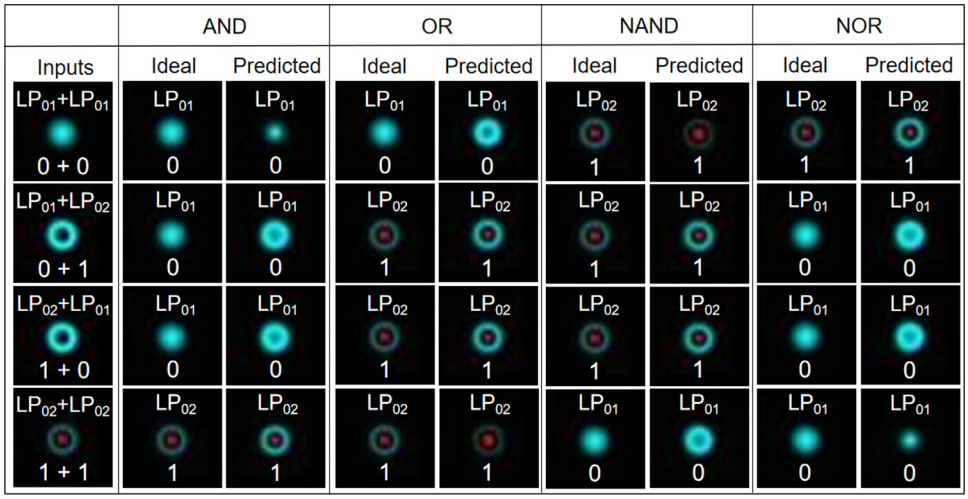

FIG. 3. Modulation results of the D^{2}NN with the AND, OR, NAND, and NOR logical operations.

the logical operation, is computed as the ratio of the predicted output's total energy to that of the input beam, i.e.,

$$E = \frac{\sum_{i=1}^{n}\sum_{j=1}^{n} e_{Oij}^2}{\sum_{i=1}^{n}\sum_{j=1}^{n} e_{Iij}^2}, \tag{8}$$

where n represents the number of pixels on the diffractive layer, O_{ij} signifies the value of a pixel on the predicted output image, and I_{ij} stands for the value of a pixel on the input image.

Concurrently, we assessed the matching quality between the predicted output and the ideal output by evaluating the structural similarity (S_{SIM}) of the predicted output. The S_{SIM} serves as a measure of mode purity, reflecting the prediction accuracy of the model, which is expressed as

$$S_{\mathrm{SIM}}(x,y) = \frac{(2\mu_x\mu_y + C_1)(2\sigma_{xy} + C_2)}{(\mu_x^2 + \mu_y^2 + C_1)(\sigma_x^2 + \sigma_y^2 + C_2)}, \tag{9}$$

where x and y denote the predicted output image and the ideal output image, respectively, μ_x and μ_y represent the mean brightness of the two images, respectively, σ_x and σ_y stand for the standard deviations of the brightness of the two images, respectively, σ_{xy} represents the covariance of the brightness between the two images, and C_1 and C_2 are constant terms used to stabilize the denominator.

The obtained light field on the receiving screen exhibits the expected LP mode and replicates the same light field distribution as the ideal output mode, boasting a diffraction efficiency of over 98% and a mode purity exceeding 97%. Subsequently, we trained the D^{2}NN model using the same input data to achieve the logical OR operation, wherein the output LP mode adheres to $Y = A + B$. Moreover, we continued training a three-layer D^{2}NN to modulate LP modes, enabling the implementation of NAND and NOR operations. In these cases, the output LP modes adhere to $Y_{\mathrm{NAND}} = \overline{AB}$ and $Y_{\mathrm{NOR}} = \overline{A + B}$, respectively. Figure 3 showcases the modulation results of the OR, NAND, and NOR gates, while Fig. 4 illustrates the diffraction efficiency and mode purity of these logical operations.

The NOT gate represents a distinct type of logic gate characterized by only two input states: "0" and "1". Therefore, the crux of the logical NOT operation is to switch between LP_{01} and LP_{02} modes. Figure 5(a) illustrates the modulation results of the "NOT" operation. Here, we constructed a three-layer D^{2}NN to train the NOT gate. The input of the model only contains two LP modes (i.e., LP_{01} and LP_{02}), and NOT logical operations aim to exchange the two modes. Figure 5(b) exhibits a diffraction efficiency exceeding 98% and a mode purity exceeding 99% for these two logical operations, underscoring the performance of the designed D^{2}NN model in executing logical NOT operations on LP modes.

XNOR and XOR gates represent more intricate logic operations that can be constructed by sequentially combining basic AND, OR, and NOT gates [42]. Utilizing LP_{01} and LP_{02} as the logical variables A and B, respectively, the outcomes for XNOR and XOR gates are consistently defined. To accomplish this, we trained a three-layer D^{2}NN to modulate LP modes for executing logic operations in the sequence of AND, NOT, and then OR. The input for the OR function is derived from the outcomes of the cascaded AND and NOT gates, enabling the realization of XNOR and XOR logic. Figure 6 illustrates an LP mode-based XOR gate implemented via cascaded logic operations, with the XNOR gate functioning similarly. It is crucial to account for potential additional transmission losses and coupling losses between modes resulting from these cascaded operations, as these could impact separability and operational efficiency. Figure 7 reveals that the diffraction efficiencies for these two logic operations exceed 70%,

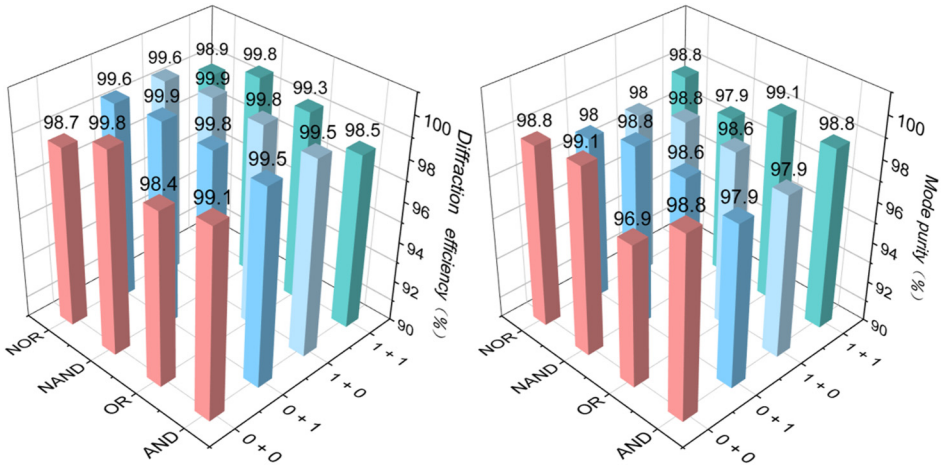

FIG. 4. Diffraction efficiency and mode purity of the AND, OR, NAND, and NOR logical operations.

and the mode purities surpass 96%, underscoring the efficacy of our D^{2}NN design in conducting cascade logical operations on LP modes. Reflecting on the earlier training results, the D^{2}NN exhibits precise modulation of LP mode conversions across all input scenarios, confirming its utility as a versatile instrument for the efficient and autonomous modulation of diverse light fields, thereby underscoring its proficiency in facilitating fundamental logical operations.

Conventional optoelectronic systems encounter conversion losses when optical signals transition to electrical signals, attributed to the involvement of optical and electronic components. In addition, phenomena such as scattering, absorption, refraction of light, and transmission losses in optical fibers or alternative waveguides can diminish the intensity of the optical signals. This reduction compromises signal quality and the overall performance of the system. The advent of digital computing in optoelectronics might also precipitate energy dissipation in the manipulation and control of optical signals, with losses emanating from factors such as material absorption, the architectural design of devices, and imperfections in optical properties. For instance, elementary optical logic operations employing compact silicon for phase modulation in silicon waveguides and incident beams [43] can experience an average energy loss exceeding 50%, primarily due to transmission and photoelectric conversion inefficiencies in the waveguide. In contrast, our proposed three-layer D^{2}NN method leverages interference and diffraction operations to facilitate LP mode logic operations without necessitating signal conversion, thereby circumventing the photoelectric conversion and device energy losses typical of conventional approaches. Our findings reveal that the energy loss associated with five basic logic operations (AND, OR, NOT, NAND, and NOR) is under 5%, and the energy loss for cascading logic operations (XNOR and XOR) remains below 30%. The logic strategy we have developed significantly enhances energy efficiency and system performance, offering a viable solution for reducing energy consumption in optical computing and optical information processing.

For the three-layer diffraction structure, we consider that the multiplane light conversion system composed of multiple cascaded spatial light modulators may be a suitable device for experimental implementation. Spatial light modulators (SLMs), functioning as quasiplanar

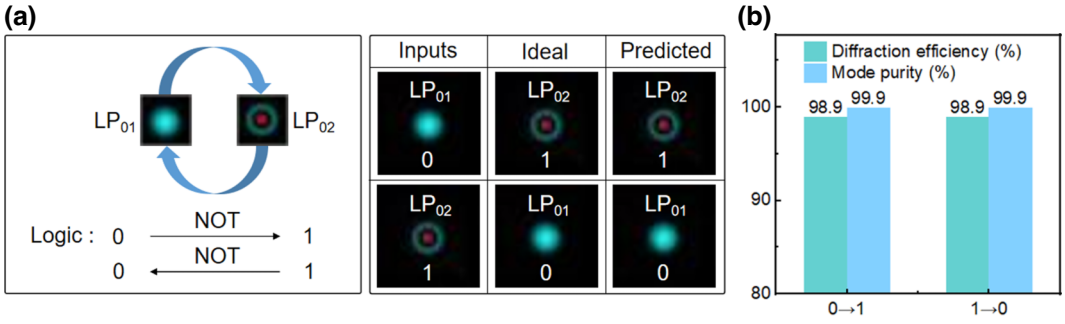

FIG. 5. Result of the LP mode logic "NOT" operation. (a) Modulation results of the "NOT" operation. (b) Diffraction efficiency and mode purity of the NOT logical operation.

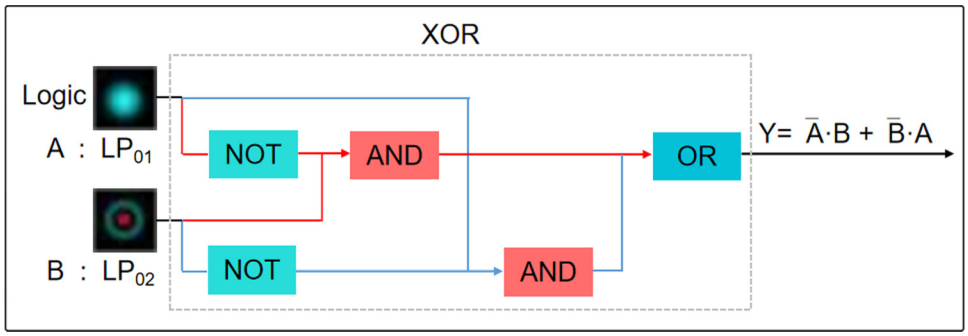

FIG. 6. Logical XOR gate based on the cascaded LP mode operation.

devices, facilitate the modulation of amplitude and phase distributions across wave fronts. By properly aligning a cascade of SLMs, it becomes feasible to mimic the modulation processes characteristic of three-layer diffractive structures. For example, such three-layer diffractive structures have been advocated for showcasing high-dimensional quantum gates for OAM modes, utilizing cascaded SLMs [44]. Moreover, considering the spatially nonuniform optical field configurations inherent to both LP and OAM modes, the integration of multiple SLMs could enable the construction of three-layer diffraction modulation. This approach holds promise for executing LP logic operations effectively.

IV. DISCUSSION

Optical logic operations traditionally rely on on-chip modulation, using light intensity as the input signal and controlling the logic output through the chip's optical configuration. Yet, the creation of intricate logic circuits could result in significant power consumption and thermal management challenges, attributed to the constrained parallelism and inherent properties of electronic components. This complexity elevates both the cost and intricacy of the system. For example, AND logic operations via phase modulation in silicon waveguides typically achieve a diffraction efficiency of less than 50%, limiting their utility in optical computing due to excessive energy demands [43]. Conversely, recent advancements in free-space modulation techniques, particularly those employing the D^2NN, have shown promising outcomes in executing logic operations [13,45]. Our multilayer diffraction approach has demonstrated the capacity to attain a diffraction efficiency of 70% when facilitating AND logic gates. Notably, our D^2NN-based approach to LP mode logic operations achieves a remarkable diffraction efficiency

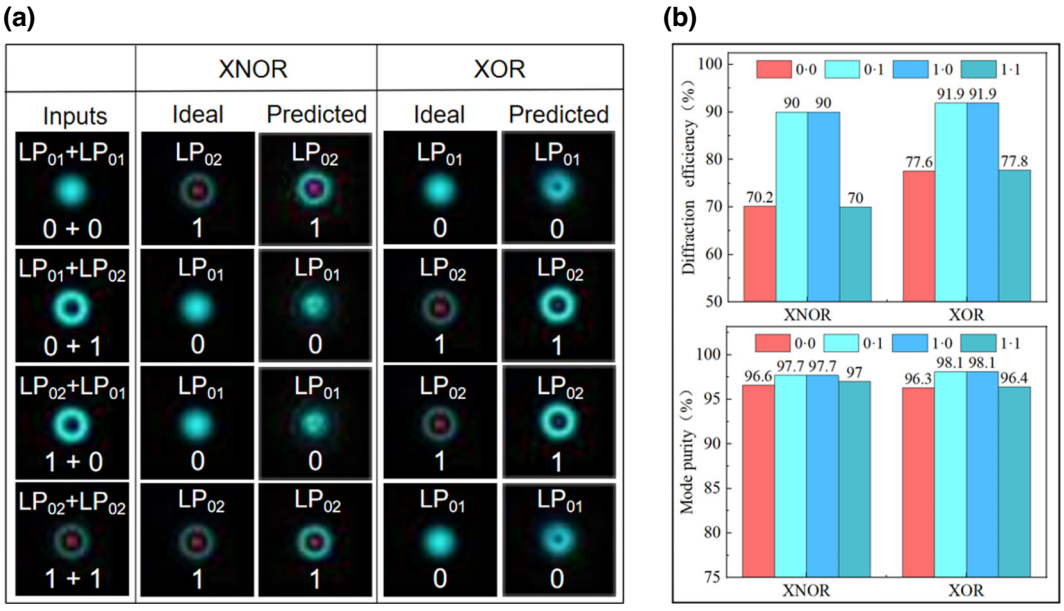

FIG. 7. Results of the cascaded LP mode logical operations based on the D^2NN. (a) Modulation results of the D^2NN with the XNOR and XOR logical integration operations. (b) Diffraction efficiency and mode purity of the XNOR and XOR logical integration operations.

exceeding 98% and a mode purity of 97%. Moreover, the inherent orthogonality of the LP modes affords additional degrees of freedom in modulation, enabling the execution of complex and high-order logic operations as well as the integration of multiple logic functions. This demonstrates that our LP mode-focused logic strategy can serve as a versatile technique for the efficient and independent modulation of multiple optical fields, capable of executing fundamental logical operations.

The LP modes exhibit distinct differences in both phase and intensity distributions. Leveraging LP modes as the foundation for logic states enables the execution of precise and sophisticated logic operations. In comparison with conventional optical logic gates reliant on intensity-based states, logic operations facilitated by the LP modes of the D^2NN enable independent modulation of input light field distributions, markedly reducing energy loss and significantly enhancing computational speed and anti-interference capabilities in logic operations. Beyond accomplishing the aforementioned seven logic gates, the exceptional information processing capability of the D^2NN allows for the utilization of any LP mode as a logic state, enabling the realization of high-order logic operations that pose challenges for traditional optical logic operations.

To validate the efficacy of the D^2NN model in high-order LP mode logical operations, we explored logical operations among these advanced LP modes. Given constraints imposed by the number of LP modes generated by the incident laser wavelength, core radius, core refractive index, and cladding refractive index, we selected multiple high-order LP modes from the available finite LP modes for validation and presented one of the outcomes. Specifically, we designated the high-order LP_{41} mode as the logical state "0" and the LP_{42} mode as the logical state "1". Employing the same methodology as previously described, we conducted AND and OR gates logical operations. In addition, we delved into the integration of logical AND and OR operations involving high-order LP modes: LP_{02}, LP_{03}, LP_{11}, and LP_{12}. We used LP_{02} and LP_{03} for logical AND operations and LP_{11} and LP_{12} for logical OR operations, resulting in eight input states. Employing the previously established methodology, we constructed a three-layer D^2NN model that independently modulates eight input fields entering from the center of the diffraction layer. Based on phase modulation and diffraction transmission through three optical diffraction layers, we derived the predicted output results of the logical AND gate and OR gate models.

The data presented above illustrates that despite certain distortions in the intensity distributions of output optical fields during the discussed high-order LP mode logical operations, the logical functions were entirely achieved. With a diffraction efficiency surpassing 82% and a mode purity exceeding 97%, these distortions did not hamper the execution of logical operations using high-order LP modes as logical states. These results demonstrate that the LP mode logical operation approach, rooted in the D^2NN as proposed in this paper, effectively accomplishes complex logical operations with high-order modes, significantly enhancing the representation capability of logical states.

V. CONCLUSION

This paper introduces and investigates an LP mode logical operation method based on the D^2NN model. Leveraging the orthogonality, robust discrimination, and anti-interference features of LP modes as logic states facilitates comprehensive optical logic functions. This approach significantly mitigates energy loss during logic operations and yields high-precision results. To independently modulate multiple input optical fields required for LP mode logic, we devised a D^2NN framework that integrates optical diffraction theory and deep learning technology. This framework establishes an approximate linear mapping relationship between diffraction layer neurons and solves multiplane diffraction structures through a three-layer phase modulation. Simulation results demonstrate that the proposed D^2NN model adeptly addresses the linear system response of multiple optical fields, accurately executing seven logical operations. Furthermore, we explore the implementation of high-order LP mode logical operations based on the D^2NN. The findings indicate that linear operations on high-order LP modes significantly curtail energy loss in logic operations and accurately achieve the integration of diverse logic operation functions. In summary, the proposed logic design method holds promise as an efficient approach for optical digital computing, offering high parallel processing capabilities.

ACKNOWLEDGMENTS

This work was funded by the National Natural Science Foundation of China (62271322, 62275162), Guangdong Basic and Applied Basic Research Foundation (2021A1515011762, 2022A1515011003, 2023A15150 30152), Shenzhen Fundamental Research Program (JCYJ 20200109144001800, JCYJ20210324095610027, JCYJ 20210324095611030), Shenzhen Universities Stabilization Support Program (SZWD2021013), Shenzhen Peacock Plan (20180921273B, 20180521645C), and Natural Science Foundation of Top Talent of SZTU (GDRC202204).

APPENDIX A: CONSTRUCTION PRINCIPLE OF THE D^2NN

The D^2NN represents a novel iteration of deep neural networks that capitalizes on diffraction principles for computational tasks. It employs optical components to

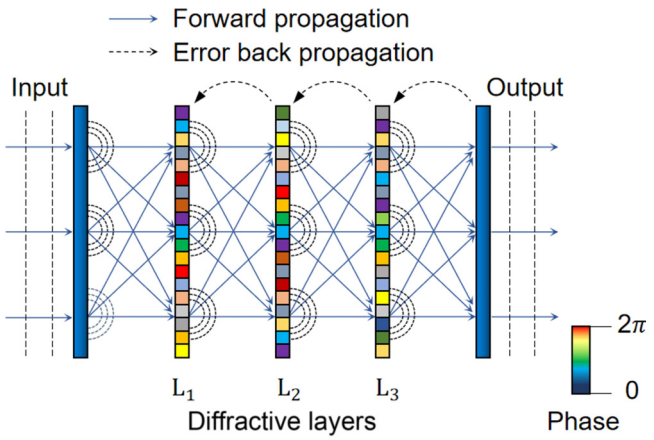

FIG. 8. Schematic of the construction of the D^{2}NN.

orchestrate the interference and diffraction of light, facilitating the forward propagation and computational processes inherent to neural networks. In contrast, traditional DNN architectures depend on electronic computing, leveraging hardware such as CPUs or GPUs to perform matrix multiplications and execute nonlinear activation functions. The D^{2}NN stands out by offering significant advantages in terms of parallelism, energy efficiency, and computational speed. Owing to the natural parallel transmission capabilities of light waves, the D^{2}NN can process numerous inputs and weights concurrently. This feature empowers the D^{2}NN to support extensive, energy-efficient, high-velocity parallel computing, distinguishing it from its traditional counterparts.

We construct the D^{2}NN model by integrating the forward propagation model based on scalar diffraction theory in optics with the error backpropagation algorithm, aimed at minimizing the loss function. As illustrated in Fig. 8, this model comprises an input layer, three optical diffractive layers, and an output layer. All of these are based on the Fresnel diffraction principle, where the colored blocks represent different phase distributions of the diffractive neurons and are fully connected to the subsequent layers through free-space optical forward propagation. The connections between these diffractive layers are established through the weights (i.e., the transmission or reflection coefficients) of each neuron, influencing the forward propagation of light. To optimize the weights of the network, we employ the error backpropagation algorithm, which adjusts these weights through phase modulation of the light waves. The algorithm is founded on the stochastic gradient descent method commonly used in traditional deep learning. Specifically, we update the phase values of light by altering the pixel sizes on the diffractive layers, allowing for complex wave front modulation. This method can achieve the predicted output of the model at a fast computing speed and low power consumption.

With the forward propagation model obeying the scalar diffraction principle and the error backward propagation model aimed to minimize the loss function, the D^{2}NN can accurately calculate the parameters and construct the desired multilayer diffractive structure, performing target modulation functions on the input light field. To assess the performance of the D^{2}NN, we establish a loss function to quantify the variance between the predicted output Y_{pred} and the actual target Y_{true}, which is represented as

$$L_{(y_{\text{true}}-y_{\text{pred}})} = \sum_{i=1}^{n} |y_{\text{true}} - y_{\text{pred}}|^2, \tag{A1}$$

where n represents the number of pixels in the diffraction layer, specifically set at 200×200 (corresponding to a layer size of 200×200 mm), and there is a distance of 300 mm between the layers. For the construction and training of the D^{2}NN model, we utilize PYTHON 3.10.4 along with GOOGLE TENSORFLOW 2.9.1. The training process was conducted using an Intel Core i7-8750H graphics processing unit with a learning rate of 0.01. Training a three-layer D^{2}NN through 5000 iterations required approximately 4 min.

APPENDIX B: HIGH-ORDER LP MODE LOGIC OPERATION BASED ON THE D^{2}NN

The LP mode can be expressed as $E_{lm}(r,\varphi)$ in a step-index optical fiber. The latter is a type of optical fiber with a step-index refractive index distribution. The refractive index of the fiber core is higher than that of the cladding, and the refractive index distribution is uniform. This allows the input light to propagate continuously through total internal reflection at the interface between the core and cladding. When the refractive index difference between the core and cladding of a step-index optical fiber is much less than one, this type of fiber is called a weakly guiding fiber. The transmitted light waves in it are linearly polarized, and the fiber modes are linearly polarized modes, also called LP modes [46–49]. We call this mode "LP$_{lm}$", where the subscripts l and m relate to the intensity distribution pattern of the LP$_{lm}$ mode (the modal field); l is the azimuthal index, which indicates the maximum number of intensity cycles per revolution ($\varphi = 360°$) and m is the radial index, which reveals the number of modal fields from the core to the cladding along the r-direction. Therefore, the LP$_{lm}$ mode can be expressed as follows:

$$E_{LP} = E_{lm}(r,\varphi)\exp[j\,(\omega t - \beta_{lm} z)], \tag{B1}$$

where E_{LP} represents the electric field of the LP mode and β_{lm} is the propagation constant along the z-direction.

The number of propagating modes in an optical fiber depends on the normalized frequency parameter V of the transmitted light waves. The normalized frequency parameter V depends on the incident laser wavelength λ, the core

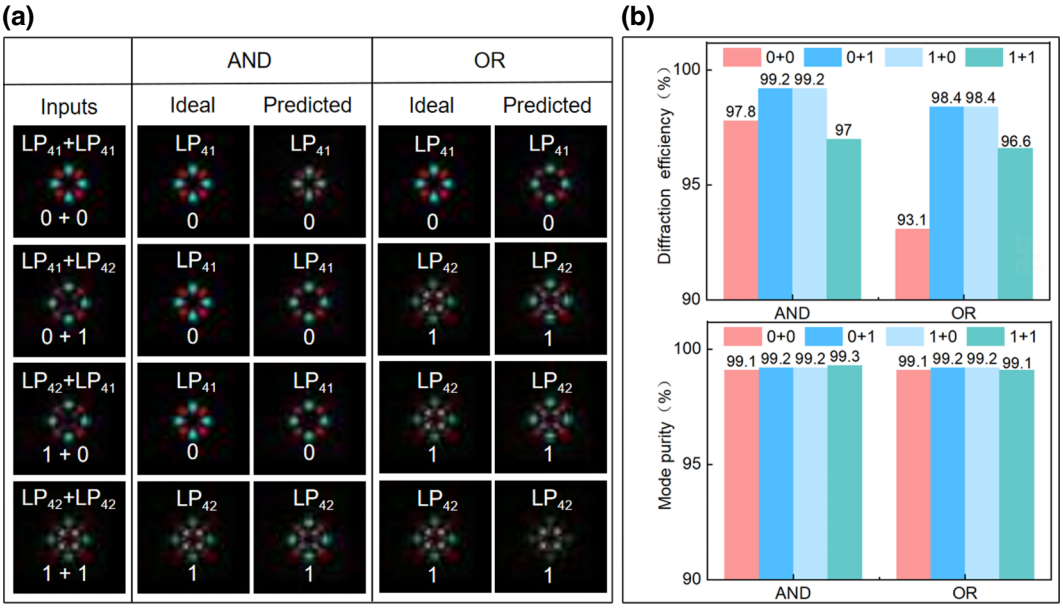

FIG. 9. Results of the high-order LP mode logic operations based on the D^{2}NN. (a) Modulation results of the D^{2}NN with the AND and OR logical operations. (b) Diffraction efficiency and mode purity of the AND and OR logical operations.

radius α, the core refractive index n_{core}, and the cladding refractive index n_{cladding}, that is,

$$V = \frac{2\pi\alpha}{\lambda}\sqrt{n_{\text{core}}^2 - n_{\text{cladding}}^2}. \tag{B2}$$

When $V < 2.405$, $2.405 \le V \le 3.832$, and $V > 3.832$, light waves excite in the optical fibers in the form of an LP_{01} mode, an LP_{11} mode, and a higher-order LP mode, respectively. We use a laser beam with a working wavelength of 1550 nm, a beam waist radius of 0.45 mm, a core refractive index of 1.43, a cladding refractive index of 1.42, and a core radius of 15 nm. Finally, 15 LP modes are produced through an optical fiber and, according to operational requirements, we finally select LP_{41} and LP_{42} to represent logical constants "0" and "1". Employing the same methodology as described previously, we conducted AND and OR gate logical operations, showcasing the outcomes in Fig. 9(a). Figure 9(b) illustrates the diffraction

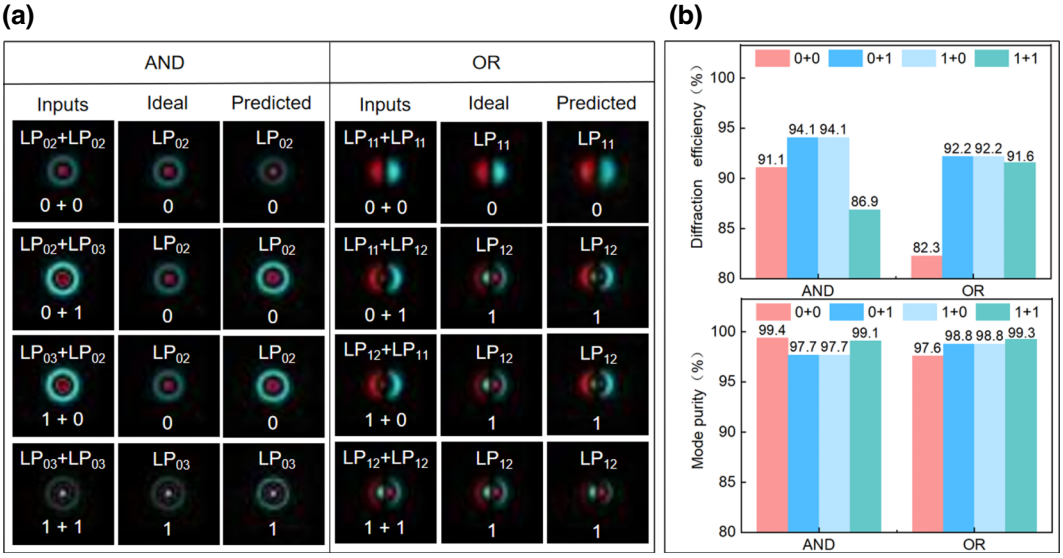

FIG. 10. Results of the high-order LP mode logical integration operations based on the D^{2}NN. (a) Modulation results of the D^{2}NN with the AND and OR logical integration operations. (b) Diffraction efficiency and mode purity of the AND and OR logical integration operations.

efficiency and mode purity of the AND and OR logical operations.

APPENDIX C: LOGICAL INTEGRATION OF THE HIGH-ORDER LP MODES

To validate the efficacy of the D^2NN model for high-order LP mode logical operations, we also explored logical integration operations among the following LP modes: LP_{02}, LP_{03}, LP_{11}, and LP_{12}. We utilized two logical variables, A and B, to denote LP_{02} and LP_{03}, respectively, setting LP_{02} as logical state "0" and LP_{03} as logical state "1". Executing the logical AND operation, $Y = AB$, results in four distinct input states. Similarly, we employed two logical variables, C and D, to represent LP_{11} and LP_{12}, with LP_{11} as logical state "0" and LP_{12} as logical state "1". Carrying out the logical OR operation, $Y = C + D$, yields a total of eight input states. Employing the previously established methodology, we constructed a three-layer D^2NN model, independently modulating the eight input fields entering from the center of the diffraction layer. Following the phase modulation and diffraction transmission through three optical diffraction layers, we derived the predicted output results of the model for the logical AND and OR gates. The integration of the logical operations for high-order LP modes is illustrated in Fig. 10(a). Figure 10(b) illustrates the diffraction efficiency and mode purity for the AND and OR logical integration operations.

APPENDIX D: PERFORMANCE OF THE LP MODE LOGIC OPERATIONS BASED ON THE D^2NN

We present two approaches to examine the correlation between the necessary neuron count and mask dimensions within a specifically designed three-layer dense diffraction neural network. The dimension of each diffraction layer's mask is determined by $L = uN \times uN$, where u represents the length of a neural unit and N signifies the pixel count. In the initial method, we maintain a constant N across each diffraction layer while adjusting u in the D^2NN model to showcase the logical AND operation. The resulting trends in the output diffraction efficiency and mode purity are depicted in Fig. 11. Notably, both the diffraction efficiency and mode purity exhibit a gradual decline as u decreases. This observation highlights that diminishing the dimensions of neural units leads to a reduced neuron density per unit area, adversely impacting the volume of the input information captured. Consequently, this diminution directly affects the model's efficacy in information transmission and processing.

In the second scenario, we hold u constant and iterate the logical AND operation by varying N to forecast the diffraction efficiency and mode purity of the outcome. As depicted in Fig. 12, these metrics progressively improve with an increase in N, eventually reaching a plateau. This trend suggests that an increase in N can enhance the predicted output quality. A larger N leads to a higher resolution, enabling the neural networks to discern more subtle features and patterns. This enhancement in resolution contributes to the accuracy and overall quality of the predictions. In addition, a greater N expands the imaging area, which mitigates noise interference and boosts the signal-to-noise ratio. Nonetheless, this improvement arises at the cost of increased memory requirements and extended training durations for model optimization, presenting a notable tradeoff.

When employing LP modes predicted by the D^2NN for cascaded logic gate inputs, it is crucial to account for error accumulation from their repeated usage. The prediction error from each gate cumulatively affects the output of subsequent gates. To assess this, we initiated the output from an AND gate as an input for another AND gate. Precisely, outputs resembling the previous logic "0 + 0" and "1 + 1" were redefined as the new logic 0 and 1, respectively. This redefined logic "0" and "1" served as inputs for another iteration of the AND operation. This new predicted output maintained over 87% diffraction efficiency and 95% mode purity. This method of cascaded training

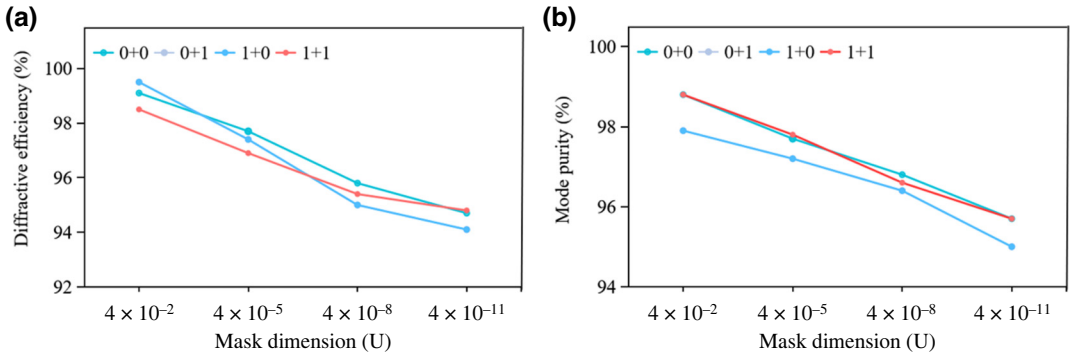

FIG. 11. Results of predicted output changes with mask dimension. Here, U is the mask dimension. (a) Changes in diffraction efficiency of the logical AND gates. (b) Changes in mode purity of the logical AND gates.

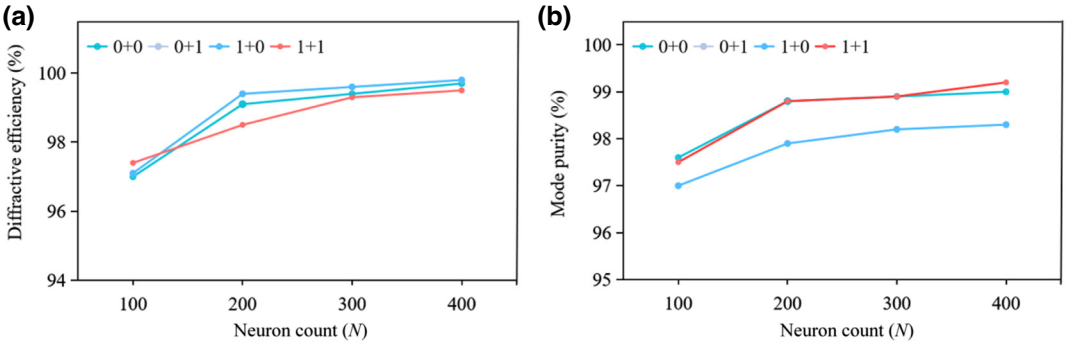

FIG. 12. Results of the predicted output changes with neuron count. Here, N is the neuron count. (a) Changes in diffraction efficiency of the logical AND gates. (b) Changes in mode purity of the logical AND gates.

and evaluation was iteratively performed. Figure 13(a) illustrates the modulation outcomes from several cascaded AND logic operations.

According to the simulations displayed in Fig. 13(b), when setting the information loss threshold at 5%, the LP modes predicted by the D^2NN can be reliably reused up to four times as inputs for other logic gates before experiencing a reduction in diffraction efficiencies at below 50% and mode purities at below 80%. These simulation findings confirm that our D^2NN model is capable of executing repeated logical operations within a permissible margin of error.

APPENDIX E: ON-CHIP APPLICATIONS OF FREE-SPACE LOGIC OPERATIONS

On-chip logic operations traditionally utilize light intensity as the input signal, modulating logic outputs via the chip's optical architecture for effective integration [50,51]. However, the creation of complex logic circuits can result in elevated power consumption and thermal dissipation challenges. These arise from the constraints on parallelism and the inherent physical properties of electronic components, thereby escalating system complexity and costs. Furthermore, on-chip logic operations face challenges in executing large-scale parallel computations concurrently, which can limit computational efficiency for certain tasks. In contrast, the LP mode logic operations enabled by the D^2NN are categorized under free-space logic operations. These leverage the interference and diffraction properties of light waves for computation and information processing in an unconfined space. Free-space logic operations boast superior parallelism, reduced energy consumption, and enhanced capacity for optical signal processing when compared with conventional on-chip methods. This approach not only supports the inclusion of a greater

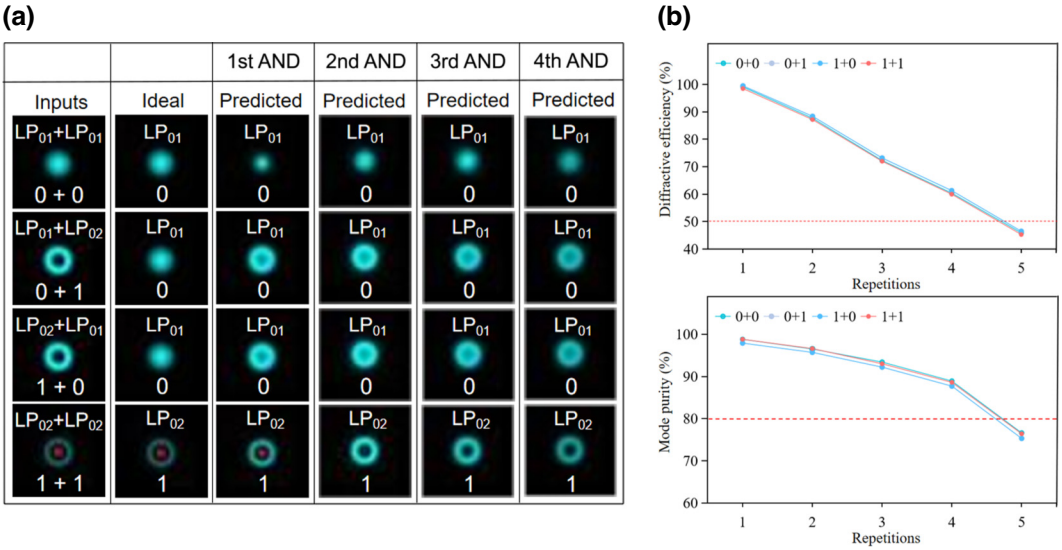

FIG. 13. Results of the multiple cascaded AND logical operations based on the D^2NN. (a) Modulation results of the D^2NN with the cascaded AND logical integration operations. (b) Changes in diffraction efficiency and mode purity of the cascaded AND logical operations. The red dashed horizontal lines on the graphs indicate the minimum thresholds for diffraction efficiency and mode purity required to prevent information loss.

number of orthogonal modes for processing extensive data and executing complex logic tasks simultaneously but also capitalizes on the low-loss and high-throughput attributes of light transmission to facilitate energy-efficient calculations.

In addition, the miniaturization potential of the D^2NN is inherently constrained by the minimal optical numerical aperture and the spacing between diffraction layers. The numerical aperture in optical instruments is a critical factor that influences the system's optical resolution and sensitivity. A reduced optical numerical aperture is capable of delivering enhanced resolution and more refined optical characteristics. Nonetheless, when endeavoring to miniaturize the D^2NN, the fabrication of optical components with smaller numerical apertures encounters challenges due to the current limitations of manufacturing technologies and the properties of materials used. Such challenges stem from the fact that reducing numerical apertures can significantly elevate manufacturing expenses and complicate the production process. Moreover, the separation between diffraction layers is dictated by the physical dimensions of the device, with the manufacturing process restrictions making it challenging to accommodate higher computational densities and more sophisticated optical functionalities within a limited space. Concurrently, reduced layer spacing may intensify mutual interference and coupling among light waves, necessitating more meticulous design and optimization efforts. However, with ongoing advancements in manufacturing and integration technologies of optical devices, it is anticipated that these physical constraints will gradually diminish, facilitating the advancement of the D^2NN toward compact integration.

[1] H. Wei, Z. Wang, X. Tian, M. Käll, and H. Xu, Cascaded logic gates in nanophotonic plasmon networks, Nat. Commun. **2**, 1 (2011).

[2] Y. Fu, X. Hu, C. Lu, S. Yue, H. Yang, and Q. Gong, All-optical logic gates based on nanoscale plasmonic slot waveguides, Nano Lett. **12**, 5784 (2012).

[3] J. M. Jeong and M. E. Marhic, All-optical logic gates based on cross-phase modulation in a nonlinear fiber interferometer, Opt. Commun. **85**, 430 (1991).

[4] R. G. A. Craig, G. S. Buller, F. A. P. Tooley, S. D. Smith, A. C. Walker, and B. S. Wherrett, All-optical programmable logic gate, Appl. Opt. **14**, 2148 (1990).

[5] A. A. Sawchuk and T. C. Strand, Digital optical computing, Proc. IEEE **72**, 758 (1984).

[6] H. J. Caulfield and S. Dolev, Why future super computing requires optics, Nat. Photonics **4**, 261 (2010).

[7] D. Woods and T. J. Naughton, Optical computing, Appl. Math. Comput. **215**, 1417 (2009).

[8] J. Touch, A.-H. Badawy, and V. J. Sorger, Optical computing, Nanophotonics **6**, 503 (2017).

[9] Z. Huang, Y. He, P. Wang, W. Xiong, H. Wu, J. Liu, H. Ye, Y. Li, D. Fan, and S. Chen, Orbital angular momentum deep multiplexing holography via an optical diffractive neural network, Opt. Express **30** (4), 5569 (2022).

[10] W. Xiong, Z. Huang, P. Wang, X. Wang, Y. He, C. Wang, J. Liu, H. Ye, D. Fan, and S. Chen, Optical diffractive deep neural network-based orbital angular momentum mode add–drop multiplexer, Opt. Express **29** (22), 36936 (2021).

[11] M. S. S. Rahman and A. Ozcan, Time-lapse image classification using a diffractive neural network, Adv. Intell. Syst. **5** (5), 2200387 (2023).

[12] Z. Gu, Y. Gao, and X. Liu, Optronic convolutional neural networks of multi-layers with different functions executed in optics for image classification, Opt. Express **29**, 5877 (2021).

[13] C. Qian, X. Lin, X. Lin, J. Xu, Y. Sun, E. Li, B. Zhang, and H. Chen, Performing optical logic operations by a diffractive neural network, Light: Sci. Appl. **9**, 59 (2020).

[14] Y. Sang, X. Wu, S. S. Raja, C. Y. Wang, H. Li, Y. Ding, D. Liu, J. Zhou, H. Ahn, and S. Gwo, Broadband multifunctional plasmonic logic gates, Adv. Opt. Mater. **6**, 1701368 (2018).

[15] H. Liu, Z. Quan, Y. Cheng, S. Deng, and L. Yuan, Ultracompact universal linear-optical logic gate based on single rectangle plasmonic slot nanoantenna, Plasmonics **16**, 1 (2021).

[16] A. Pal, M. Z. Ahmed, and S. Swarnakar, An optimized design of all-optical XOR, OR, and NOT gates using plasmonic waveguide, Opt. Quantum Electron. **53**, 84 (2021).

[17] M. W. McCutcheon, G. W. Rieger, J. F. Young, D. Dalacu, P. J. Poole, and R. L. Williams, All-optical conditional logic with a nonlinear photonic crystal nanocavity, Appl. Phys. Lett. **95**, 221102 (2009).

[18] Q. Xu and M. Lipson, All-optical logic based on silicon micro-ring resonators, Opt. Express **15**, 924 (2007).

[19] Q. Zhao, S. Hao, Y. Wang, L. Wang, and C. Xu, Orbital angular momentum detection based on diffractive deep neural network, Opt. Commun. **443**, 245 (2019).

[20] Z. Wang, C. Qian, Z. Fan, and H. Chen, Arbitrary polarization readout with dual-channel neuro-metasurfaces, Adv. Sci. **10** (5), 2204699 (2023).

[21] C. Qian, Z. Wang, H. Qian, T. Cai, B. Zheng, X. Lin, Y. Shen, I. Kaminer, E. Li, and H. Chen, Dynamic recognition and mirage using neuro-metamaterials, Nat. Commun. **13** (1), 2694 (2022).

[22] P. Wang, W. Xiong, Z. Huang, Y. He, Z. Xie, J. Liu, H. Ye, Y. Li, D. Fan, and S. Chen, Orbital angular momentum mode logical operation using optical diffractive neural network, Photonics Res. **9** (10), 2116 (2021).

[23] Z. Zhao, Y. Wang, X. Ding, H. Li, J. Fu, K. Zhang, S. N. Burokur, and Q. Wu, Compact logic operator utilizing a single-layer metasurface, Photonics Res. **10** (2), 316 (2022).

[24] X. Lin, Y. Rivenson, N. T. Yardimci, M. Veli, Y. Luo, M. Jarrahi, and A. Ozcan, All-optical machine learning using diffractive deep neural networks, Science **361**, 1004 (2018).

[25] T. Yan, J. Wu, T. Zhou, H. Xie, F. Xu, J. Fan, L. Fang, X. Lin, and Q. Dai, Fourier-space diffractive deep neural network, Phys. Rev. Lett. **123**, 023901 (2019).

[26] T. Zhou, X. Lin, J. Wu, Y. Chen, H. Xie, Y. Li, J. Fan, H. Wu, L. Fang, and Q. Dai, Large-scale neuromorphic optoelectronic computing with a reconfigurable diffractive processing unit, Nat. Photonics **15**, 367 (2021).

[27] M. Veli, D. Mengu, N. T. Yardimci, Y. Luo, J. Li, Y. Rivenson, M. Jarrahi, and A. Ozcan, Terahertz pulse shaping using diffractive surfaces, Nat. Commun. **12**, 37 (2021).

[28] J. Shi, D. Wei, C. Hu, M. Chen, K. Liu, J. Luo, and X. Zhang, Robust light beam diffractive shaping based on a kind of compact all-optical neural network, Opt. Express **29**, 7084 (2021).

[29] M. Zheng, L. Shi, and J. Zi, Optimize performance of a diffractive neural network by controlling the Fresnel number, Photonics Res. **10**, 2667 (2018).

[30] D. Mengu, Y. Luo, Y. Rivenson, and A. Ozcan, Analysis of diffractive optical neural networks and their integration with electronic neural networks, IEEE J. Sel. Top. Quantum Electron. **26**, 3700114 (2019).

[31] H. Chen, J. Feng, M. Jiang, Y. Wang, J. Lin, J. Tan, and P. Jin, Diffractive deep neural networks at visible wavelengths, Engineering **7** (10), 1483 (2021).

[32] S. Jiao, J. Feng, Y. Gao, T. Lei, Z. Xie, and X. Yuan, Optical machine learning with incoherent light and a single-pixel detector, Opt. Lett. **44**, 5186 (2019).

[33] Z. Wu and Z. Yu, Small object recognition with trainable lens, APL Photonics **6**, 071301 (2021).

[34] Y. LeCun, Y. Bengio, and G. Hinton, Deep learning, Nature **521**, 436 (2015).

[35] J. Schmidhuber, Deep learning in neural networks: an overview, Neural Networks **61**, 85 (2015).

[36] Q. Zhang, H. Yu, M. Barbiero, B. Wang, and M. Gu, Artificial neural networks enabled by nanophotonics, Light: Sci. Appl. **8**, 1 (2019).

[37] R. Zhu, T. Qiu, J. Wang, S. Sui, C. Hao, T. Liu, Y. Li, M. Feng, A. Zhang, and C. Qiu, Phase-to-pattern inverse design paradigm for fast realization of functional metasurfaces via transfer learning, Nat. Commun. **12**, 1 (2021).

[38] H. Ren, W. Shao, Y. Li, F. Salim, and M. Gu, Three-dimensional vectorial holography based on machine learning inverse design, Sci. Adv. **6**, eaaz4261 (2020).

[39] Z. Huang, P. Wang, J. Liu, W. Xiong, Y. He, J. Xiao, H. Ye, Y. Li, S. Chen, and D. Fan, All-optical signal processing of vortex beams with diffractive deep neural networks, Phys. Rev. Appl. **15** (1), 014037 (2021).

[40] Z. Huang, P. Wang, J. Liu, W. Xiong, Y. He, X. Zhou, J. Xiao, Y. Li, S. Chen, and D. Fan, Identification of hybrid orbital angular momentum modes with deep feedforward neural network, Results Phys. **15**, 102790 (2019).

[41] P. Wang, W. Xiong, Z. Huang, Y. He, J. Liu, H. Ye, J. Xiao, Y. Li, D. Fan, and S. Chen, Diffractive deep neural network for optical orbital angular momentum multiplexing and demultiplexing, IEEE J. Sel. Top. Quantum Electron. **28** (4), 1 (2022).

[42] D. A. B. Miller, Are optical transistors the logical next step?, Nat. Photonics **4** (1), 3 (2010).

[43] A. Kotb and C. Yao, All-optical logic operations based on silicon-on-insulator waveguides, Opt. Eng. **62** (4), 048101 (2023).

[44] F. Brandt, M. Hiekkamäki, F. Bouchard, M. Huber, and R. Fickler, High-dimensional quantum gates using full-field spatial modes of photons, Optica **7** (2), 98 (2020).

[45] X. Lin, K. Zhang, K. Liao, H. Huang, Y. Fu, X. Zhang, S. Feng, and X. Hu, Polarization-based all-optical logic gates using diffractive neural networks, J. Opt. **26** (3), 035701 (2024).

[46] J. R. Qian and W. P. Huang, LP modes and ideal modes on optical fibers, J. Lightwave Technol. **4**, 626 (1986).

[47] B. Crosignani, C. H. Papas, and P. Di Porto, Coupled-mode theory approach to nonlinear pulse propagation in optical fibers, Opt. Lett. **6**, 61 (1981).

[48] B. Bendow, P. D. Gianino, N. Tzoar, and M. Jain, Theory of nonlinear pulse propagation in optical waveguides, J. Opt. Soc. Am. **70** (5), 539 (1980).

[49] Z. Fang, Y. Yao, K. Xia, M. Kang, K. I. Ueda, and J. Li, Vector mode excitation in few-mode fiber by controlling incident polarization, Opt. Commun. **294**, 177 (2013).

[50] L. He, F. Zhang, H. Zhang, L.-J. Kong, W. Zhang, X. Xu, and X. Zhang, Topology-optimized ultracompact all-optical logic devices on silicon photonic platforms, ACS Photonics **9** (2), 597 (2022).

[51] Q. Tan, C. Qian, and H. Chen, Inverse-designed metamaterials for on-chip combinational optical logic circuit, Prog. Electromagn. Res. **176**, 55 (2023).